

Observation of ubiquitous charge correlations and hidden quantum critical point in hole-doped kagome superconductors

Ilija K. Nikolov,¹ Giuseppe Allodi,² Adrien Rosuel,^{1,3} Ginevra Corsale,^{1,4} Anshu Kataria,² Pietro Bonfà,⁵ Roberto De Renzi,² Andrea Capa Salinas,⁶ Stephen D. Wilson,⁶ Marc-Henri Julien,⁷ Samuele Sanna,⁴ and Vesna F. Mitrović^{1,3,*}

¹*Department of Physics, Brown University, Providence, Rhode Island 02912, USA*

²*Dipartimento di Scienze Matematiche, Fisiche e Informatiche, Università di Parma, I-43124 Parma, Italy*

³*Brown Center for Theoretical Physics and Innovation,*

BCTPI, Brown University, Providence, RI 02912-1843, USA

⁴*Dipartimento di Fisica e Astronomia, Università di Bologna, I-40127 Bologna, Italy*

⁵*Dipartimento di Fisica, Informatica e Matematica,*

Università di Modena e Reggio Emilia, Via Campi 213/a, 41125 Modena, Italy

⁶*Materials Department, University of California Santa Barbara, Santa Barbara, California 93106, USA*

⁷*Université Grenoble Alpes, Laboratoire National des Champs Magnétiques Intenses, CNRS,*

Université de Toulouse, INSA Toulouse, European Magnetic Field Laboratory, 38042 Grenoble, France

(Dated: December 11, 2025)

The interplay between superconductivity and charge-density wave (CDW) order, and its evolution with carrier density, is central to the physics of many quantum materials, notably high- T_c cuprates and kagome metals. Hole-doped kagome compounds exhibit puzzling double-dome superconductivity and, as chemical substitution inevitably introduces quenched disorder, their properties remain poorly understood. Here, by leveraging the sensitivity of nuclear quadrupole resonance to local and static orderings, we uncover new features, primarily the incipient and fragmented CDW phases, in the charge landscape of $\text{CsV}_3\text{Sb}_{5-x}\text{Sn}_x$. Static CDW puddles are observed well above the transition temperature, a hallmark of pinning by defects. Their doping and temperature evolution indicate that, in the absence of disorder, the inverse Star-of-David π -shifted (ISD- π) CDW order would vanish near $x = 0.12$, between the two superconducting domes. This critical doping represents a hidden quantum critical point. Nevertheless, the ISD- π pattern persists well beyond previous reports, although its volume fraction is progressively reduced up to the critical doping at which it saturates. We establish that carrier doping promotes fragmentation of the ISD- π order, whereas randomness preserves the ISD- π patches.

Understanding the multifaceted nature of the relationship between charge density wave (CDW) and superconductivity (SC) is a major open question in condensed matter physics [1]. Since both originate from effective attractive electron-electron interactions, they often compete but may coexist, or even enhance each other. Understanding their complex interplay can provide valuable insight into the mechanisms driving unconventional SC. The presence of disorder further complicates the physics to the extent that it can produce notable changes in the morphology of phase diagrams ([2, 3] and refs. therein).

The prototypical materials of such complex physics are cuprate superconductors, where despite over three decades of research, the interplay between SC and CDW has yet to be fully understood [1]. An even greater complexity marks the family of vanadium-based $A\text{V}_3\text{Sb}_5$ ($A = \text{K}, \text{Rb}, \text{Cs}$) kagome superconductors [4] due to the mixing of topologically nontrivial bands with structures that promote strong electronic correlations, *i.e.*, flat bands and Dirac cones [5–14]. In particular, CsV_3Sb_5 has not fallen short of promise and exhibits a wide range of electronic instabilities, including 3Q CDW order [15–18] before reaching a SC ground state [4]. The mechanism

behind SC still remains a mystery, with proposals ranging from phonon-driven pairing to CDW and current-loop fluctuations [4]. In order to understand how electronic instabilities govern the interplay between CDW and SC, one can tune the Fermi level by means of carrier doping and hydrostatic pressure.

Studies on hole-doped CsV_3Sb_5 have suggested that the CDW order disappears to give way to double-dome SC [19–22]. Doping inherently introduces defects into the lattice, which may disrupt CDW and/or alter SC. This has sparked debates about the intrinsic role of quenched disorder in shaping the CDW character even in archetypal materials [3]. An important question is whether CDW is sensitive to disorder, which in turn modifies SC, or whether both are independently affected. In kagome systems, where topology, frustration, and strong interactions lead to exotic properties [4], the question becomes even more relevant. Untangling these effects from disorder is thus essential for understanding what fundamentally underpins the physics of kagome materials.

To identify the complex interaction between CDW, SC and disorder, as well as eliminate possible magnetic-field-induced artifacts, we employ nuclear quadrupole resonance (NQR) on high-quality $\text{CsV}_3\text{Sb}_{5-x}\text{Sn}_x$ powders [23]. NQR is a local probe whose response comes from the bulk and is sensitive to static effects. More

* corresponding author: vemi@brown.edu

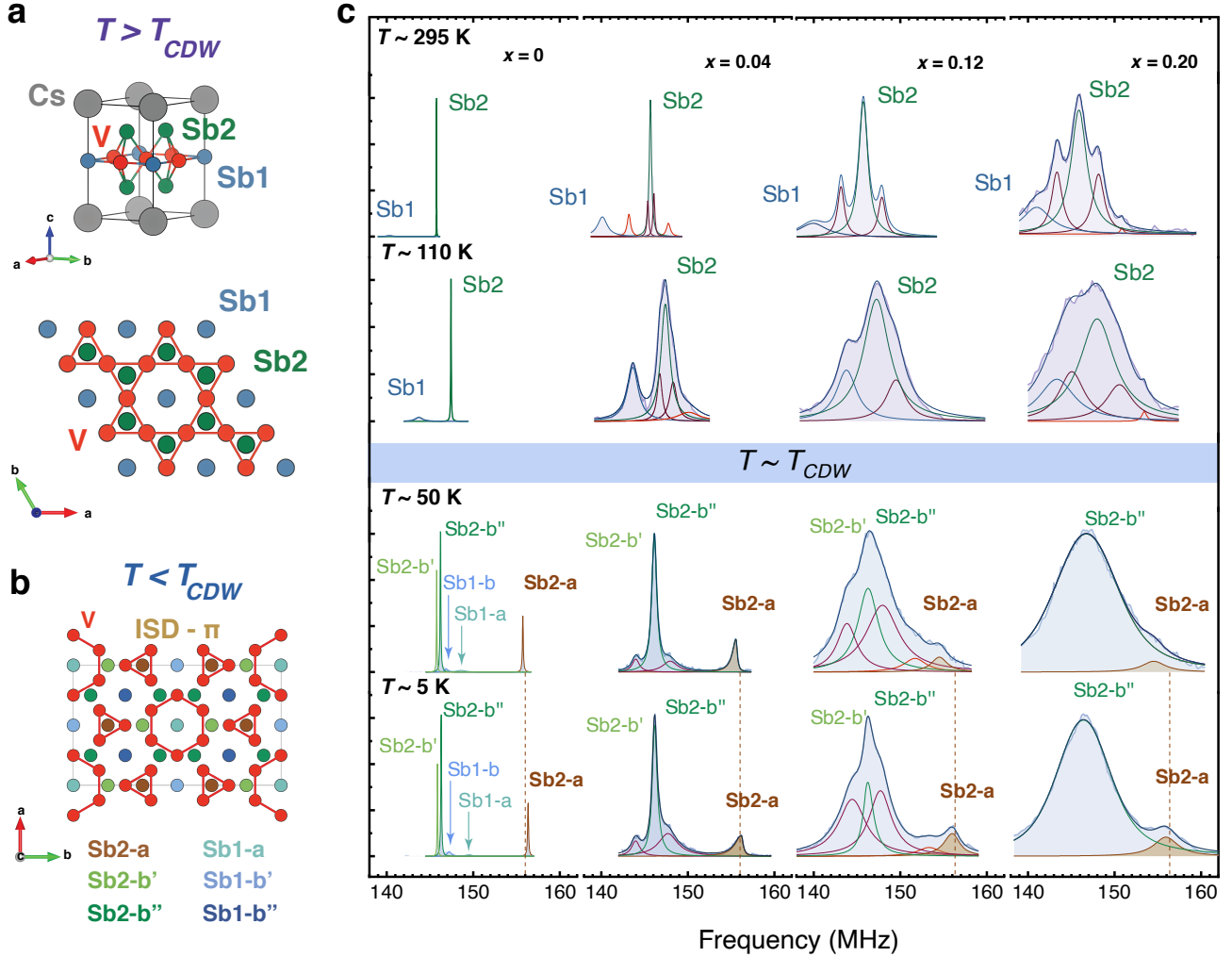


FIG. 1. **Commensurate inverse Star-of-David CDW.** (a) Crystallographic structure of CsV_3Sb_5 in the pristine phase. The kagome pattern is realized by the V atom in red. We distinguish two Sb sites: the basal Sb1 site, blue, and the apical Sb2 site, green. (b) Crystallographic structure of CsV_3Sb_5 below T_{CDW} . The hexagonal lattice becomes orthorhombic with an inverse Star-of-David π -shifted modulation (ISD- π) (c) NQR ^{121}Sb spectra for the $5/2 \rightarrow 3/2$ transition as a function of temperature and Sn-doping x in $\text{CsV}_3\text{Sb}_{5-x}\text{Sn}_x$. The solid curves represent Lorentzian-based models, while the data is the shaded color area. Even at high Sn-doping, charge ordering T_{CDW} is unambiguously determined by the presence of the Sb2-a peak (brown curve) at approximately 156 MHz. For the undoped sample, below T_{CDW} , the whole sample is in the ISD- π phase. The Sb1-a and Sb1-b = Sb1-b' & Sb1-b'' peaks are omitted for $x \geq 0.04$. The extra room temperature peaks belong to the Sb2 site based on site-occupancy analysis and dopant-induced neighboring-site effects.

importantly, since local magnetism (except the putative loop-current in the CDW [4]) is absent in these compounds, NQR uniquely probes the charge density in the ground state. The power of this technique to determine the microscopic nature of the charge density ordering was demonstrated in RbV_3Sb_5 [24]. Here, we apply the same methodology on the hole-doped $\text{CsV}_3\text{Sb}_{5-x}\text{Sn}_x$ compounds and find that the lattice instability for $x = 0$ is the inverse star of David, π -shifted along the c -axis (ISD- π), also known as staggered trihexagonal. We establish that this leading CDW instability (ISD- π) survives up to at least $x = 0.35$, corresponding to the maximum of the second SC dome, and that the local CDW amplitude remains largely unchanged. The dominant ef-

fect of the dopant is to fragment the parent ISD- π order.

Interestingly, at high temperatures, well above the transition temperature into the CDW order (T_{CDW}), we detect nucleation of local static modulations of the charge density, *i.e.* CDW “puddles.” These puddles, present at all temperatures above T_{CDW} , arise from charge correlations once they are pinned by disorder. Moreover, the T -dependence of the correlations reveals a doping-tuned QCP that lies at the end of the first SC dome. The QCP indicates the critical doping at which the CDW would be suppressed in the absence of quenched disorder.

Nature of CDW in doped kagome lattice. The kagome pattern in CsV_3Sb_5 is realized by the vana-

dium atoms (Fig. 1a & b) forming a quasi-2D structure. The Sn-substitution of similarly sized Sb-atoms, amounting to hole doping, is achieved with minimal steric hindrance [19]. In the pristine phase, above T_{CDW} , the system has two inequivalent antimony sites, Sb1 basal, center of V hexagons, and Sb2 apical, center of V triangles.

The ^{121}Sb nucleus (spin number $I = 5/2$) has a finite quadrupole moment that couples to the electric field gradient (EFG) formed by the surrounding charge distribution. This coupling makes ^{121}Sb NQR a very sensitive probe of local charge arrangements. Because no ordered magnetism was detected in CsV_3Sb_5 [4], the ^{121}Sb NQR observables can be directly related to the EFG. A particular peak in the NQR spectrum corresponds to a ^{121}Sb site in the unit cell, whereas the area under the peak (spectral area) is proportional to its occupancy in the unit cell (see Methods).

We first discuss the NQR spectra of the undoped sample, CsV_3Sb_5 , shown in Fig. 1c. At room temperature, the two sites are easily discernible with the area ratio of (Sb1 : Sb2 = 1 : 4), in agreement with their respective site occupancies. When the temperature is reduced, $T < T_{\text{CDW}}$, the transition to the CDW phase is clearly identifiable by the appearance of the Sb2-a peak at higher frequencies, Fig. 1c. Following the procedure described in detail in Ref. [24], we associate the appearance of the Sb2-a peak with the emergence of the inverse Star-of-David (ISD) distortion pattern. As shown in Fig. 1b, the ISD pattern is realized on an orthorhombic unit cell and breaks the in-plane rotational symmetry. In addition, the Sb2-b peak splits into two spectral lines (Fig. 1b & c), which represents the hallmark of the π -shifted ISD [24]. The ISD- π pattern is marked by the staggering of layers of ISD that are π shifted relative to neighboring layers along the c -axis within a $2\times 2\times 2$ supercell.

Next, we turn to NQR spectra analysis of the doped $\text{CsV}_3\text{Sb}_{5-x}\text{Sn}_x$ for $T < T_{\text{CDW}}$. There are two features in the NQR spectra, the appearance of the Sb2-a site and the splitting of Sb2-b, that allow us to determine the microscopic nature of CDW. First, we detect the Sb2-a site for all doping levels, as depicted in light-brown shaded regions in Fig. 1c. The presence of the Sb2-a site indicates that the ISD order persists up to the highest doping level investigated here ($x = 0.35$). Second, the splitting of Sb2-b into two additional sites that provides conclusive evidence for the π -shifted ISD is clearly perceptible only for doping levels up to $x = 0.12$, as illustrated in Fig. 1c and Supplementary Note III. For $x \geq 0.20$, the splitting of the Sb2-b peak is not distinguishable due to excess spectral broadening. Nevertheless, the broadening does not impede us from determining whether interlayer correlations, *i.e.*, π shift between neighboring layers, are present in the ISD-CDW phase.

Examining the spectral features enables us to extract the order parameter of the ISD-CDW, defined as the Sb2-a frequency, and its volume fraction, corresponding to the spectral area. In Fig. 2a we plot the CDW order parameter as a function of temperature for the different

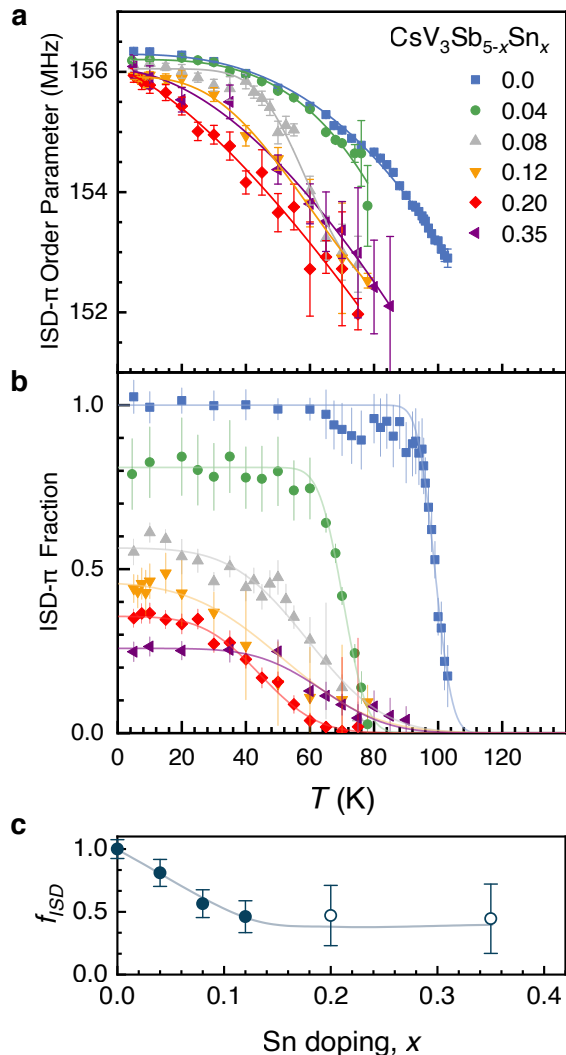


FIG. 2. **CDW order parameter.** (a) The frequency of the Sb2-a site is proportional to the amplitude of the CDW modulation. The minimal change in the low temperature Sb2-a frequency shows that the CDW amplitude is almost unaltered by the dopant. (b) The ISD- π volume fraction as a function of temperature. (c) The low-temperature volume-fraction (f_{CDW}) as a function of Sn-doping shows that the ISD- π survives in at least half of the sample. Open symbols are for data calculated by two techniques (Supplementary Note II). Error bars represent two standard deviations and are not shown when smaller than the symbol.

doping levels. We observe that, for all doping levels, the order parameter reaches nearly the same frequency as the temperature approaches zero. Measurements in the undoped sample, where the spectral features are sharp, demonstrate that the frequency difference between the two Sb2 sites is only compatible with ISD- π [24]. As doping increases, we find that the frequency difference between the two sites only slightly decreases. Therefore, as the frequency difference remains nearly unchanged with doping, we conclude that the ISD- π pattern survives.

To further probe the nature of the CDW as a function of doping, we examine the volume fraction of ISD- π , de-

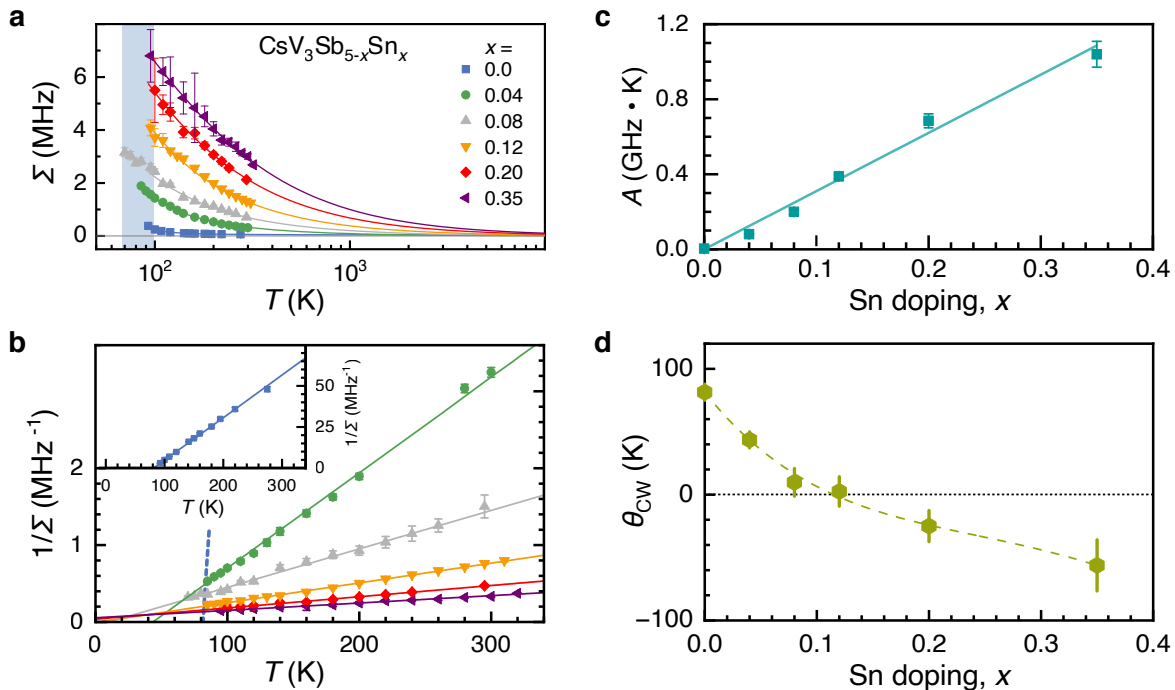


FIG. 3. **High-temperature charge correlations.** (a) Full-width-at-half-maximum (Σ) of the dominant Sb2 peak in the pristine phase $T > T_{\text{CDW}}$. The blue-shaded area represents the T_{CDW} range for different dopings. (b) Linear fit to $1/\Sigma$ demonstrates the Curie-Weiss (CW) behavior of the pristine-phase Sb2 linewidth and directly shows the intersection with the x -axis. The solid lines are CW fits. The inset is the undoped data. The dashed line is the CW fit of the undoped compound. Note that the undoped compound is a pure crystal as opposed to doped samples which are powders. (c) The doping dependence of the CW parameter A shows that Sn-doping is linearly proportional to the intrinsic CDW features. (d) The CW temperature extracted from the linear fit shows a sign change in the vicinity of $x = 0.12$. The dashed green line is a guide to the eye. Error bars represent two standard deviations and are not shown when they are smaller than the symbol size.

terminated as the ratio between the spectral area under the Sb2-a peak and the total spectral area. We plot the T -dependence of the volume fraction and its value extrapolated at $T = 0$ (f_{ISD}) in Figs. 2b and c, respectively. The results show that f_{ISD} is progressively reduced as a function of doping and saturates in the vicinity of 50%. In other words, the ISD order persists up to the highest doping level investigated but occupies no more than 50% of the sample. Thus, the system stabilizes in an inhomogeneous configuration in which the ISD- π order is fragmented. Additionally, recent XRD measurements deduced a drastic reduction in the correlation length at $x = 0.025$ for a 2×2 CDW in the plane [16]. Together, these results affirm that the CDW is short-range, consistent with our fragmentation picture. Another key effect of dopant-induced fragmentation is the inevitable suppression of interlayer correlations, *i.e.*, the π -shift, without changing the nature of the CDW itself. Thus, the size of the fragment controls whether π -shift is present.

An open question remains as to the exact nature of the additional phase (remaining 50% of volume fraction) that coexists with the ISD- π order at finite doping levels. With the aim of answering the question, we simulate NQR spectra corresponding to different CDW patterns proposed in previous work [15, 16, 25–29] and compare them with the measured spectra (Supple-

mentary Note VII). These patterns include the $2a_0$ [25], $4a_0$ [15, 16, 25], $\frac{3}{8}a_0$ [27], $3a_0$ [28] and incommensurate CDW [16, 26] on the hexagonal, $Fm\bar{3}m$ and $C2m$ phases. Surprisingly, all of the potential charge arrangements explain equally well the spectral lineshape. Therefore, we cannot indisputably conclude which of the other proposed phases coexist with ISD- π at finite doping. Nonetheless, we establish that the presence of a layer of Star-of-David (SoD) [30] and/or alternating stacking of SoD and ISD layers [31] is incompatible with our findings (Supplementary Note VI).

High-temperature charge correlations. To better understand the CDW emergence, we proceed to analyze ^{121}Sb NQR spectral details at higher temperatures ($T > T_{\text{CDW}}$). We find that NQR spectra feature linewidth broadening with a particular temperature evolution. Because in these compounds, $\text{CsV}_3\text{Sb}_{5-x}\text{Sn}_x$, there is no ordered magnetism [4], the broadening comes from the local charge distribution. From the linewidth, we extract the full-width-at-half-maximum (Σ) of the Sb2 peak and plot it in Fig. 3a as a function of temperature, $T > T_{\text{CDW}}$, for all doping levels. The Σ follows a Curie-Weiss (CW) increase down to T_{CDW} . The solid line in

Fig. 3a depicts a fit to the Curie-Weiss law

$$\Sigma(T) = \frac{A}{T - \theta_{CW}} + C, \quad (1)$$

where θ_{CW} is the CW temperature, C is the infinite- T linewidth, and A is related to both the correlation length and maximum amplitude of the CDW modulation.

The pre-transitional broadening of the NQR/NMR linewidth in CDW systems is a well-documented effect [26, 32–35]. Specifically, in the archetypal compound of charge ordering, NbSe₂, this broadening was associated with the formation of static short-range regions (puddles) of the incipient CDW [32]. The universality of the broadening in CDW compounds is illustrated in Fig. S10. Furthermore, a similar effect has recently been observed in STM ([36] and refs. therein).

The emergence of puddles for $T > T_{CDW}$ appears naturally in realistic metals that inevitably contain impurities. Around them, Friedel oscillations occur, predominantly at the CDW wave vector if it exists. Quenched disorder can pin the fluctuations associated with these oscillations, inducing static components, *i.e.*, puddles of incipient CDW, that locally break the pristine translational symmetry. This manifests itself in the NQR spectrum via linewidth broadening induced by local distortions that change the EFG around the nuclear active site. On approaching T_{CDW} , the volume fraction of the incipient CDW grows as illustrated in Fig. 4d-f causing a further increase in the NQR linewidth as observed in Fig. 3.

To extract the parameters of the CW law, we plot $1/\Sigma(T)$ in Fig. 3b. Our fit finds that C is zero within the error bar (± 0.1 MHz), suggesting that besides CDW pinning, the linewidth broadening is not strongly affected by Sn-doping. That is, doping does not appreciably distort the crystallographic structure so that it could introduce a significant distribution of EFG parameters. This finding ($C \approx 0$) is somewhat unusual because EFGs are quite sensitive to disorder and thus doped compounds would have broader lines in the high-temperature limit. Furthermore, in Fig. 3c, we plot the parameter A as a function of doping. More disorder means that there are more pinning sites at high temperatures, thus an increase of A . In the nominally undoped compound, A remains finite but extremely small compared to that of the doped materials, which is an indication of the good quality of the undoped sample.

The divergence in the CDW susceptibility is characterized by extracting the CW temperature, θ_{CW} , as a function of doping (Fig. 3d). This intrinsic CDW susceptibility, following the CW T -dependence, is exclusively associated with electronic degrees of freedom. In other words, it is dissociated from randomness/disorder effects. The θ_{CW} exhibits a clear change of sign in the vicinity of $x = 0.12$ doping and describes the growth of CDW fluctuations pinned by disorder, *i.e.*, puddles, as the system tends to order. Remarkably, while θ_{CW} changes sign at $x \approx 0.1$, Fig. 3d, for $T < T_{CDW}$ the CDW persists, as ev-

idenced by both its order parameter and volume fraction (Fig. 2). This implies that CDW would be suppressed at $x \approx 0.12$ if no quenched disorder were present in the system. In the absence of quenched disorder, the sole effect of doping is to tune the Fermi level [19]. Therefore, the electronic ground state becomes unfavorable to CDW formation for doping levels exceeding $x \approx 0.12$, where $\theta_{CW} \leq 0$. However, the detection of short-range CDW up to $x = 0.35$ establishes the crucial role of disorder, *i.e.*, intrinsic randomness of Sn-dopants, in stabilizing the CDW. In particular, the short-range CDW order survives as a result of fragmentation enabled by disorder. Thus, $x \approx 0.12$ represents a critical doping where a putative quantum critical point (QCP) hidden by disorder and possibly SC is harbored. This result is comparable to the one found in recent coherent phonon spectroscopy experiments, indicating that the critical doping (location of QCP) is independent of the energy scale of the probe [28, 37]. Even for temperatures below T_{CDW} , there is a notable change of the CDW phase at this critical doping. More precisely, while we observe that f_{ISD} saturates at 50 %, the addition of disorder does not change the nature of CDW (Fig. 2). Furthermore, at the critical doping, there is an abrupt change in the width of the CDW transition (Fig. S11). Therefore, beyond the critical doping, the salient order is the fragmented ISD- π .

Next, we address the disordered character of the CDW phase transition. The identification of the incipient CDW order reveals that puddles of short-ranged CDW exist far above T_{CDW} . Our findings are in agreement with other techniques that detect dynamical responses in CsV₃Sb₅ [22, 26, 37–42]. Specifically, recent x-ray diffraction measurements concluded that the CDW in CsV₃Sb₅ is of the order-disorder type with a critical growth of quasi-static domains [39]. Such quasi-static domains would be revealed in NQR spectral measurements only if they contain truly static components. Therefore, the presence of the incipient CDW, as identified by NQR, demonstrates that these fluctuations encompass static contributions.

Hole-doping phase diagram. A comprehensive phase diagram for CsV₃Sb_{5-x}Sn_x as a function of hole doping in Fig. 4 maps out the boundaries of various charge orderings. Looking first at the ISD- π order parameter in Fig. 2, we extract the transition temperature of the CDW transition, T_{CDW} . What is more, the spectral area corresponding to the order parameter is used to establish ISD- π volume fraction, f_{ISD} (Fig. 2b). By overlaying the volume fraction, the CW temperature and the SC transition temperature (T_c) as a function of doping, we reveal that the critical doping, corresponding to the hidden QCP ($x \approx 0.12$), coincides with the saturation point of the ISD- π volume fraction, and lies between the two SC domes. Moreover, we find that beyond this doping level ($x \gtrsim 0.12$), the subsisting order is the fragmented ISD- π . We point out that between the long-range and fragmented order, there must be a second-

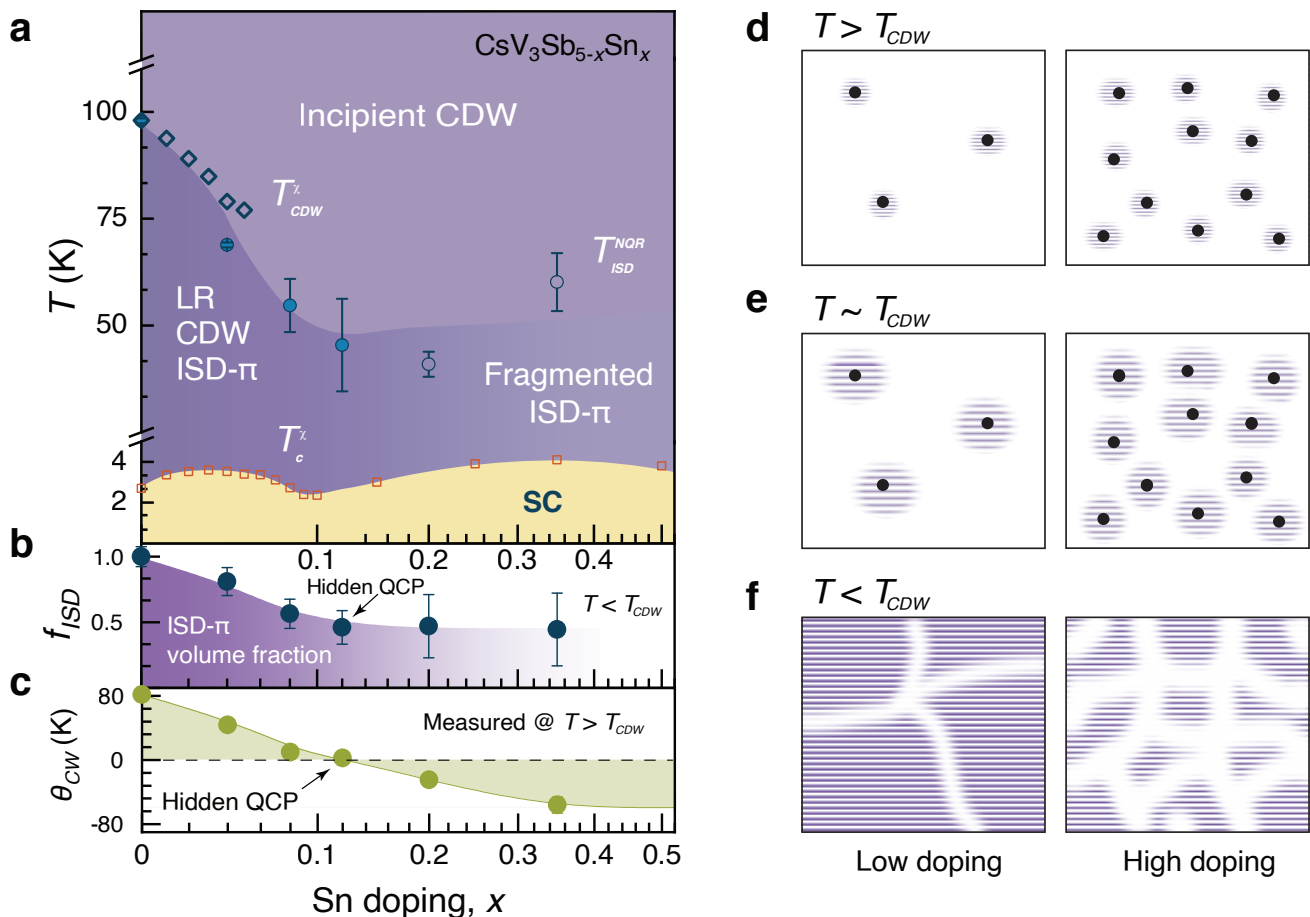


FIG. 4. **Temperature phase diagram of $\text{CsV}_3\text{Sb}_{5-x}\text{Sn}_x$ as a function of Sn-doping.** (a) Incipient CDW exists in the high temperature region, $T > T_{CDW}$. The ISD- π onset temperature is denoted by T_{CDW} , where LR denotes long-range order. The gradient represents crossover between the LR and fragmented order. Open diamond and square symbols are magnetization χ measurements of the bulk CDW, dark blue, and SC, burned orange, transition temperatures, from [19]. (b) Volume fraction of ISD- π . Shown error bars reflect two standard deviations. (c) Doping-dependence of the CW temperature θ_{CW} . The value $\theta_{CW} = 0$ indicates critical doping at which a putative hidden quantum critical point (QCP) lies. Error bars not shown for clarity. Solid lines serve as a guide to the eye. (d-f) Schematic of the T -dependent formation of CDW in the presence of quenched disorder for low and high doping. Black dots represent Sn-dopants and disorder, while purple lines represent charge modulations. (d) For $T > T_{CDW}$, Friedel oscillations occur around impurities to form incipient CDW. (e) On approaching T_{CDW} , the incipient CDW spreads. (f) For $T < T_{CDW}$, long-range CDW develops at low doping, while increased doping induces domain walls (white ribbon) that fragment the parent CDW.

order phase transition in the vicinity of the critical doping that is most likely influenced by the nearby hidden QCP. At finite temperatures, fluctuations associated with the QCP could smear out such a phase transition, impeding its detection. Additionally, disorder-induced broadening of the phase transition can also obstruct its detection.

Below, we discuss the effect of disorder on CDW formation. Above T_{CDW} , puddles nucleate around disorder sites. Specifically, from the linear growth of the CW constant A with Sn-doping (Fig. 3c), we deduce that the puddles are trapped by the Sn-dopant sites that act as pinning centers, as illustrated in Fig. 4d. For a fixed doping level, we observe that the linewidth increases significantly on approaching T_{CDW} as a consequence of the spreading of the puddles around the defect, as depicted in Fig. 4e. When the puddles eventually overlap, they form the ISD- π order at $T \sim T_{CDW}$ (Fig. 4f). This scenario

neatly explains the CW temperature dependence of the zero-field CDW susceptibility, similar to the generalized susceptibility in x-ray measurements [39]. Below T_{CDW} , on the other hand, the effect of disorder is to fragment the long-range ISD- π order. Strictly speaking, each impurity slightly detunes the CDW modulations, which interfere with each other and generate domain walls (shown in white in Fig. 4f). This fragments the parent ISD- π order that becomes short-ranged beyond the critical doping. There are two ways in which defects can induce the mismatch that ultimately leads to ISD- π fragmentation. For instance, at low-doping, for long-range coherence to be established, the CDW must escape pinning and move away from the defects [36]. In an alternative scenario, another CDW of unknown nature forms around impurities, while the parent CDW forms away from the defects [43].

We now examine the role of Sn-doping in affecting in-

trinsic randomness in the kagome lattice. The CW behavior above T_{CDW} allows us to study pure electronic properties corresponding to systems free of randomness. We find that at the same critical doping determined from the analysis of θ_{CW} , there are significant changes in the properties that characterize the CDW phase below T_{CDW} (Fig. 4b). This implies that the Sn-dopants introduce intrinsic randomness and do not act as simple impurities. In other words, it is the randomness of the location distribution of the dopants that dictates the physics, even at high doping. This is consistent with recent XRD measurements on $\text{CsV}_3\text{Sb}_{5-x}\text{Sn}_x$ affirming that there is no evidence of their macroscopic clustering [16]. Nevertheless, even high-quality samples, such as the ones used here, may appear locally heterogeneous on a microscopic length-scale due to random arrangements of dopant locations.

In order to understand the intrinsic origin of the QCP, we contrast our findings with those from the pressure response. A recent NQR study uncovered a pressure-tuned QCP in the undoped CsV_3Sb_5 [26]. For pressure levels higher than that corresponding to the QCP, the CDW is entirely suppressed [25–27, 44, 45]. This is in stark contrast to our finding that the ISD CDW survives at Sn-doping levels well above the QCP. What is more, at the QCP doping level, ISD volume fraction saturates. Therefore, quenched disorder plays a major role not only in enhancing the incipient CDW and causing nucleation around Sn-dopants, but it is also essential in sustaining the ISD distortion pattern via fragmentation at high doping. While the NQR pressure study observed a CW temperature dependence of the charge susceptibility, they found no evidence of charge ordering beyond the pressure-tuned QCP [26]. This confirms our conclusion that CDW persists due to randomness of dopant distribution that drives fragmentation.

A further difference between pressure-tuned and doping-tuned QCPs is their location relative to the SC domes. The pressure-tuned QCP is at the pressure level that corresponds to the maximum of the second SC dome [25–27, 44, 45], suggesting a possible link between the CDW and SC. However, the critical doping corresponding to QCP lies in the vicinity of the minimum of T_c (Fig. 4a), and thus, naively, the QCP weakens SC. The comparison may prove difficult as the QCP found by NQR is related to pure electronic effects in the absence of disorder, while T_c was measured on samples with disorder. At a basic level, our results indicate that the CDW and SC exhibit a very complex relationship in these kagome systems. In addition, the effect of disorder may render the relationship even more intricate.

Prospective. In this work, we reveal that Sn-doping introduces holes that govern the electronic properties and intrinsic disorder due to their random locations in the lattice. As a consequence, the local ISD- π distortion pattern is identified at $T \lesssim T_{\text{CDW}}$ markedly for all Sn-doping investigated, $x \leq 0.35$. However, its volume frac-

tion and correlation length decrease as a consequence of randomness-induced fragmentation. For $T \gg T_{\text{CDW}}$, short-ranged puddles are detected. Importantly, both incipient CDW and ISD- π persist as a function of doping beyond what was previously measured, up to at least the doping level corresponding to the maximum of the second SC dome [16, 19]. It was proposed that even a small orbital-selective hole doping of the Sb bands would induce CDW renormalization, resulting in strong charge fluctuations and appearance of incommensurate, quasi-1D charge correlations preceded by the ISD- π suppression [16]. Here, we determine that ISD- π persists, albeit fragmented (short-ranged) beyond the critical doping due to disorder, which explains why it has eluded detection until now [4, 16, 19]. Our findings are consistent with recent experimental observations of doping-induced short-range CDW [20, 28, 29, 46].

In these kagome systems, shifting the Fermi level to relevant points of the Brillouin zone is predicted to promote electronic orderings, including CDW order and unconventional SC [4]. Previous theoretical studies have identified the V d orbitals and apical Sb p orbitals at the M -points as essential for the formation of saddle points, which are important for stabilizing different CDW phases [47–51]. On the other hand, the basal Sb p orbitals that form an electron-like pocket at the Γ -point have a negligible contribution to the saddle points [47–51]. Applying hydrostatic pressure causes a movement of the apical Sb sites, while Sn-doping affects mostly the basal Sb sites [19]. Although pressure suppresses local CDW order at the maximum of the second dome [4, 25, 26], here, we show that Sn-doping does not. Therefore, because Sn-doping primarily affects the Sb p orbitals at the Γ -point [19], we conclude that it is the Van Hove singularities at the M -points which are crucial for the stabilization of the CDW order, ISD- π , in these compounds.

The unveiling of the high-temperature charge correlations and local ISD- π order provides a new perspective on the complex interplay between the different types of electronic order and SC. It suggests that the nature of the SC state is different between the two domes separated by a QCP at the critical doping. Using local bulk probes, such as NQR, provides valuable information on the microscopic structure. Previous studies have found that doping suppresses the parent 3Q-CDW order [4, 16, 20, 21, 29, 52–55]. Because no local-bulk probes in the absence of magnetic field were employed in the other doping-tuned kagome compounds, it would be useful to use NQR to determine if any local CDW persists and if disorder plays a role. Overall, our results emphasize the salient role of *quenched disorder and tuning the Van Hove singularities near the M -points* in ascertaining what drives the staged electronic ordering of $\text{CsV}_3\text{Sb}_{5-x}\text{Sn}_x$. Ultimately, investigating the low-temperature state of AV_3Sb_5 kagome compounds as a function of doping through a local-bulk probe is an essential step to unravel the intricate role of disorder, topology, and charge correlations in stabilizing superconductivity.

METHODS

Sample preparation

The powder samples of $\text{CsV}_3\text{Sb}_{5-x}\text{Sn}_x$ with $x = 0, 0.04, 0.08, 0.12, 0.20, 0.35$ are prepared in exactly the same way as in the ones used in refs. [19, 23]. A single, high quality undoped CsV_3Sb_5 crystal was used for the high temperature measurements ($T > T_{\text{CDW}}$).

Nuclear quadrupole resonance (NQR)

Measurements on the powder samples were performed on a state-of-the-art, home-built phase-coherent, pulsed spectrometer at the Università di Parma. The powders were mounted on a specifically designed NQR coil in a sample holder that does not exert pressure. The measurement on the single crystal was performed on a different state-of-the-art, home-built phase-coherent, pulsed spectrometer at the LNCMI. The single crystal was mounted in a custom-built sample holder and placed under no external strain.

A typical spin echo technique is used to excite the nuclear spins similar to the one used in Ref. [24]. In NQR, the quadrupolar spins are polarized by the EFG and thus no applied magnetic field is needed. The $I = 5/2$, ^{121}Sb nuclear spin have two NQR transitions. Even though higher transitions have a lower intensity, in naturally polarized thermal ensemble of spins, the higher frequency corresponds to a higher polarization factor, which justifies using the second transition. What is more, the peak separation in the second transition is twice the one in the lower transition, resulting in a better resolution.

Details on the curve fitting analysis are given in Supplementary Note I. As the spectral intensity is related to the static local environment on a timescale of the experiment, which in our case is in the *ms* range, our measurements quantify primarily static contributions.

Sb site-occupancy in CDW phase

Guided by density functional theory (DFT) calculations described in detail in ref. [24], we estimate the effect of the structural distortion on the ^{121}Sb sites and reproduce the observed NQR spectrum. They are in a full agreement with presence of $\text{ISD-}\pi$.

The full analysis of the peak occupancy, including measurements on the first transition $1/2 \rightarrow 3/2$, indicate a perfect agreement of a single $\text{ISD-}\pi$ modulation, at all temperatures below T_{CDW} , Fig. 1c. In Tab. I we give occupancy ratios of new antimony sites that develop.

Phase	Atoms	Multiplicity
Pristine	Sb1	1
Hexagonal - P6/mmm	Sb2	4
2x2x2 CDW	Sb1-a / Sb1-b' / Sb1-b''	2 / 2 / 4
<i>Fmmm</i>	Sb2-a / Sb2-b' / Sb2-b''	8 / 8 / 16
(ISD with π shift)		

TABLE I. The ^{121}Sb atomic occupations in the CsV_3Sb_5 unit cell, with and without the $\text{ISD-}\pi$ distortion. Taken from [24]

Determination of T_{CDW}

We model the area fraction in the pristine and CDW state (Fig. 1c) with a Gaussian distribution. The relative volume fraction is described by the Gauss error function (erf), which allows to quantitatively define the CDW onset (Fig. 2):

$$1 - \text{erf}\left(\frac{T - T_0}{\sigma}\right), \quad (2)$$

where T_0 is related to the center of the distribution, and σ is related to the width of the transition temperatures. We define T_{CDW} as the temperature at which the function defined in Eq. 2 reaches 80 % of its maximum value. This allows for a consistent T_{CDW} determination and quantification of the transition width, σ .

ISD- π volume fraction calculation

To quantify $\text{ISD-}\pi$, we start by evaluating the relative area between the Sb2-a peak and the full spectrum. By comparing the extracted Sb2-a fraction with the nominal $\text{ISD-}\pi$ multiplicity expected for that site (see Table I), we determine the $\text{ISD-}\pi$ volume fraction (f_{ISD}). The volume fraction for doping levels $x = 0.20, 0.35$ is determined using two different methods, detailed in Supplementary Note I, in particular Fig. S8.

ACKNOWLEDGMENTS

We thank J. M. Kosterlitz, A. Hui, D. Feldman, I. Vinograd and A.-A. Haghighirad for helpful discussions and H. Mayaffre for help with the measurements. Work at Brown University was supported in part by the National Science Foundation grant No. DMR-1905532 and funds from Brown University and University of Bologna. Research at the LNCMI was supported in part by the Chateaubriand Fellowship of the Office for Science & Technology of the Embassy of France in the USA. SDW and ACS gratefully acknowledge support via the UC Santa Barbara NSF Quantum Foundry funded through the Q-AMASE-i program under award DMR-1906325.

AUTHOR CONTRIBUTIONS

Crystals were synthesized and characterized by A.C.S. and S.D.W. Experiments were performed by G.A., I.K.N. and G.C. Analysis of experimental results was performed by I.K.N. and G.C. I.K.N., A.R., P.B., M.H.J., S.S. and V.F.M. developed and applied the general theoretical framework. I.K.N., A.R., M.H.J., S.S. and V.F.M. lead the experimental data interpretation. V.F.M. and S.S. conceived and guided the project. All authors were involved in writing the paper.

- [1] B. Keimer, S. A. Kivelson, M. R. Norman, S. Uchida, and J. Zaanen, *Nature* **518**, 179 (2015).
- [2] H. Alloul, J. Bobroff, M. Gabay, and P. J. Hirschfeld, *Reviews of Modern Physics* **81**, 45 (2009).
- [3] R. Zhou, I. Vinograd, H. Mayaffre, J. Porras, H.-H. Kim, T. Loew, Y. Liu, M. Le Tacon, B. Keimer, and M.-H. Julien, *Physical Review Letters* **135**, 106503 (2025).
- [4] S. D. Wilson and B. R. Ortiz, *Nature Reviews Materials* **9**, 420 (2024).
- [5] Z. Li, J. Zhuang, L. Wang, H. Feng, Q. Gao, X. Xu, W. Hao, X. Wang, C. Zhang, K. Wu, S. X. Dou, L. Chen, Z. Hu, and Y. Du, *Science Advances* **4**, 10.1126/sciadv.aau4511 (2018).
- [6] N. Ghimire and I. Mazin, *Nature Materials* **19**, 137 (2020).
- [7] T. Park, M. Ye, and L. Balents, *Phys. Rev. B* **104**, 035142 (2021).
- [8] M. M. Denner, R. Thomale, and T. Neupert, *Phys. Rev. Lett.* **127**, 217601 (2021).
- [9] Y.-P. Lin and R. M. Nandkishore, *Phys. Rev. B* **104**, 045122 (2021).
- [10] M. H. Christensen, T. Birol, B. M. Andersen, and R. M. Fernandes, *Phys. Rev. B* **104**, 214513 (2021).
- [11] M. Kang, S. Fang, J.-K. Kim, B. R. Ortiz, S. H. Ryu, J. Kim, J. Yoo, G. Sangiovanni, D. Di Sante, B.-G. Park, C. Jozwiak, A. Bostwick, E. Rotenberg, E. Kaxiras, S. D. Wilson, J.-H. Park, and R. Comin, *Nature Physics* **18**, 301 (2022), publisher: Nature Publishing Group.
- [12] J.-X. Yin, B. Lian, and M. Z. Hasan, *Nature* **612**, 647 (2022).
- [13] Y. Wang, H. Wu, G. T. McCandless, J. Y. Chan, and M. N. Ali, *Nature Reviews Physics* **5**, 635 (2023).
- [14] R. Tazai, Y. Yamakawa, and H. Kontani, *Proceedings of the National Academy of Sciences* **121**, e2303476121 (2024).
- [15] H. Li, H. Zhao, B. R. Ortiz, Y. Oey, Z. Wang, S. D. Wilson, and I. Željkočić, *Nature Physics* **19**, 637 (2023).
- [16] L. Kautzsch, Y. M. Oey, H. Li, Z. Ren, B. R. Ortiz, G. Pokharel, R. Seshadri, J. Ruff, T. Kongruengkit, J. W. Harter, Z. Wang, I. Zeljkovic, and S. D. Wilson, *npj Quantum Materials* **8**, 37 (2023).
- [17] C. Guo, G. Wagner, C. Putzke, D. Chen, K. Wang, L. Zhang, M. Gutierrez-Amigo, I. Errea, M. G. Vergniory, C. Felser, M. H. Fischer, T. Neupert, and P. J. W. Moll, *Nature Physics* **20**, 579 (2024).
- [18] P. Bonfà, F. Pratt, D. Valenti, I. J. Onuorah, A. Kataria, P. J. Baker, S. Cottrell, A. C. Salinas, S. D. Wilson, Z. Guguchia, and S. Sanna, *Phys. Rev. Res.* **10.1103/bvgk-q2qn** (2025).
- [19] Y. M. Oey, B. R. Ortiz, F. Kaboudvand, J. Frassinetti, E. Garcia, R. Cong, S. Sanna, V. F. Mitrović, R. Seshadri, and S. D. Wilson, *Phys. Rev. Materials* **6**, L041801 (2022).
- [20] H. Yang, Z. Huang, Y. Zhang, Z. Zhao, J. Shi, H. Luo, L. Zhao, G. Qian, H. Tan, B. Hu, K. Zhu, Z. Lu, H. Zhang, J. Sun, J. Cheng, C. Shen, X. Lin, B. Yan, X. Zhou, Z. Wang, S. J. Pennycook, H. Chen, X. Dong, W. Zhou, and H.-J. Gao, *Science Bulletin* **67**, 2176 (2022).
- [21] Y. Sur, K.-T. Kim, S. Kim, and K. H. Kim, *Nature Communications* **14**, 3899 (2023).
- [22] G. Pokharel, C. Zhang, E. Redekop, B. R. Ortiz, A. N. C. Salinas, S. Schwarz, S. J. G. Alvarado, S. Sarker, A. F. Young, and S. D. Wilson, *Evolution of charge correlations in the hole-doped kagome superconductor $\text{CsV}_{3-x}\text{Ti}_x\text{Sb}_5$* (2025).
- [23] B. R. Ortiz, L. C. Gomes, J. R. Morey, M. Winiarski, M. Bordelon, J. S. Mangum, I. W. H. Oswald, J. A. Rodriguez-Rivera, J. R. Neilson, S. D. Wilson, E. Ertekin, T. M. McQueen, and E. S. Toberer, *Phys. Rev. Materials* **3**, 094407 (2019).
- [24] J. Frassinetti, P. Bonfà, G. Allodi, E. Garcia, R. Cong, B. R. Ortiz, S. D. Wilson, R. De Renzi, V. F. Mitrović, and S. Sanna, *Phys. Rev. Res.* **5**, L012017 (2023).
- [25] L. Zheng, Z. Wu, Y. Yang, L. Nie, M. Shan, K. Sun, D. Song, F. Yu, J. Li, D. Zhao, S. Li, B. Kang, Y. Zhou, K. Liu, Z. Xiang, J. Ying, Z. Wang, T. Wu, and X. Chen, *Nature* **611**, 682 (2022).
- [26] X. Y. Feng, Z. Zhao, J. Luo, J. Yang, A. F. Fang, H. T. Yang, H. J. Gao, R. Zhou, and G.-q. Zheng, *npj Quantum Materials* **8**, 23 (2023).
- [27] F. Stier, A.-A. Haghighirad, G. Garbarino, S. Mishra, N. Stalkerich, D. Chen, C. Shekhar, T. Laczmann, C. Felser, T. Ritschel, J. Geck, and M. Le Tacon, *Physical Review Letters* **133**, 236503 (2024).
- [28] L. Huai, Z. Wang, H. Rao, Y. Han, B. Liu, S. Yu, Y. Zhang, R. Zang, R. Luan, S. Peng, Z. Qiao, Z. Wang, J. He, T. Wu, and X. Chen, *Electronic-correlation-assisted charge stripe order in a kagome superconductor* (2025), 2509.17467.
- [29] Z. Wu, K. Sun, H. Li, L. Nie, H. Rao, D. Zhao, Z. Xiang, J. Ying, Z. Wang, T. Wu, and X. Chen, *Physical Review B* **112**, 144512 (2025).
- [30] Q. Deng, H. Tan, B. R. Ortiz, A. C. Salinas, S. D. Wilson, B. Yan, and L. Wu, *Coherent phonon pairs and rotational symmetry breaking of charge density wave order in the kagome metal CsV_3Sb_5* (2025), 2503.07442.
- [31] Y. Wang, T. Wu, Z. Li, K. Jiang, and J. Hu, *Phys. Rev. B* **107**, 184106 (2023).
- [32] B. Claude, J. D., and M. P., *Journal of Physics C: Solid State Physics* **11**, 797 (1978).
- [33] K. Ghoshray, B. Pahari, A. Ghoshray, V. V. Eremin, V. A. Sirenko, and B. H. Suits, *Journal of Physics: Condensed Matter* **21**, 155701 (2009).
- [34] T. Wu, H. Mayaffre, S. Krämer, M. Horvatić, C. Berthier, W. Hardy, R. Liang, D. Bonn, and M.-H. Julien, *Nature Communications* **6**, 6438 (2015).
- [35] I. Vinograd, R. Zhou, H. Mayaffre, S. Krämer, R. Liang, W. N. Hardy, D. A. Bonn, and M.-H. Julien, *Physical Review B* **100**, 094502 (2019).
- [36] L. Liu, C. Zhu, Z. Liu, H. Deng, X. Zhou, Y. Li, Y. Sun, X. Huang, S. Li, X. Du, Z. Wang, T. Guan, H. Mao, Y. Sui, R. Wu, J.-X. Yin, J.-G. Cheng, and S. Pan, *Physical Review Letters* **126**, 256401 (2021).
- [37] T. Kongruengkit, A. N. C. Salinas, G. Pokharel, B. R. Ortiz, S. D. Wilson, and J. W. Harter, *Persistence of charge density wave fluctuations in the absence of long-range order in a hole-doped kagome metal* (2025), 2508.13290.
- [38] Q. Chen, D. Chen, W. Schnelle, C. Felser, and B. Gaulin, *Physical Review Letters* **129**, 056401 (2022).
- [39] D. Subires, A. Korshunov, A. H. Said, L. Sánchez, B. R. Ortiz, S. D. Wilson, A. Bosak, and S. Blanco-Canosa,

- Nature Communications* **14**, 1015 (2023).
- [40] K. Yang, W. Xia, X. Mi, L. Zhang, Y. Gan, A. Wang, Y. Chai, X. Zhou, X. Yang, Y. Guo, and M. He, *Physical Review B* **107**, 184506 (2023).
- [41] Y. Zhong, T. Suzuki, H. Liu, K. Liu, Z. Nie, Y. Shi, S. Meng, B. Lv, H. Ding, T. Kanai, J. Itatani, S. Shin, and K. Okazaki, *Physical Review Research* **6**, 043328 (2024).
- [42] M. Frachet, L. Wang, W. Xia, Y. Guo, M. He, N. Maraytta, R. Heid, A.-A. Haghighirad, M. Merz, C. Meingast, and F. Hardy, *Physical Review Letters* **132**, 186001 (2024).
- [43] L. Yue, S. Xue, J. Li, W. Hu, A. Barbour, F. Zheng, L. Wang, J. Feng, S. B. Wilkins, C. Mazzoli, R. Comin, and Y. Li, *Nature Communications* **11**, 98 (2020).
- [44] K. Chen, N. Wang, Q. Yin, Y. Gu, K. Jiang, Z. Tu, C. Gong, Y. Uwatoko, J. Sun, H. Lei, J. Hu, and J.-G. Cheng, *Physical Review Letters* **126**, 247001 (2021).
- [45] H. Li, G. Fabbris, A. H. Said, J. P. Sun, Y.-X. Jiang, J.-X. Yin, Y.-Y. Pai, S. Yoon, A. R. Lupini, C. S. Nelson, Q. W. Yin, C. S. Gong, Z. J. Tu, H. C. Lei, J.-G. Cheng, M. Z. Hasan, Z. Wang, B. Yan, R. Thomale, H. N. Lee, and H. Miao, *Nature Communications* **13**, 6348 (2022).
- [46] K. J. Zhu, L. P. Nie, B. Lei, M. J. Wang, K. L. Sun, Y. Z. Deng, M. L. Tian, T. Wu, and X. H. Chen, *Physical Review Research* **6**, 023295 (2024).
- [47] H. LaBollita and A. S. Botana, *Physical Review B* **104**, 205129 (2021).
- [48] A. Tsirlin, P. Fertey, B. R. Ortiz, B. Klis, V. Merkl, M. Dressel, S. Wilson, and E. Uykur, *SciPost Physics* **12**, 049 (2022).
- [49] M. Y. Jeong, H.-J. Yang, H. S. Kim, Y. B. Kim, S. Lee, and M. J. Han, *Phys. Rev. B* **105**, 235145 (2022).
- [50] E. T. Ritz, R. M. Fernandes, and T. Birol, *Phys. Rev. B* **107**, 205131 (2023).
- [51] H. Li, X. Liu, Y. B. Kim, and H.-Y. Kee, *Physical Review B* **108**, 075102 (2023).
- [52] K. Nakayama, Y. Li, T. Kato, M. Liu, Z. Wang, T. Takahashi, Y. Yao, and T. Sato, *Physical Review X* **12**, 011001 (2022).
- [53] Y. Liu, Y. Wang, Y. Cai, Z. Hao, X.-M. Ma, L. Wang, C. Liu, J. Chen, L. Zhou, J. Wang, S. Wang, H. He, Y. Liu, S. Cui, B. Huang, J. Wang, C. Chen, and J.-W. Mei, *Physical Review Materials* **7**, 064801 (2023).
- [54] L. Huai, H. Li, Y. Han, Y. Luo, S. Peng, Z. Wei, J. Shen, B. Wang, Y. Miao, X. Sun, Z. Ou, B. Liu, X. Yu, Z. Xiang, M.-Q. Kuang, Z. Qiao, X. Chen, and J. He, *npj Quantum Materials* **9**, 23 (2024).
- [55] D. Kim, H. W. Nam, Y. Sur, K.-T. Kim, K. H. Kim, and S. J. Moon, *Physical Review B* **111**, 10.1103/physrevb.111.165151 (2025), publisher: American Physical Society (APS).